

CIRCUIT EQUATION FORMULATION OF RESISTIVE WALL MODE FEEDBACK STABILIZATION SCHEMES

M. OKABAYASHI, N. POMPHREY, R.E. HATCHER

Princeton Plasma Physics Laboratory,

Princeton University,

Princeton, New Jersey,

United States of America

ABSTRACT. Recently, various schemes for controlling the resistive wall mode have been proposed. Here, the problem of resistive wall mode feedback control is formulated utilizing concepts from electrical circuit theory. Each of the coupled elements (the perturbed plasma current, the poloidal passive shell system and the active coil system) is considered as lumped parameter electrical circuits obeying the usual laws of linear circuit theory. A dispersion relation is derived using different schemes for the feedback logic. The various schemes differ in the choice of sensor signal, which is determined by some combination of the three independent circuit currents. Feedback schemes are discussed which can, ideally, completely stabilize the kink mode. These schemes depend, for their success, on a suitable choice for the location of the sensors. A feedback scheme based on sensing the passive shell eddy current is discussed which seeks to drive the feedback system response to a point of marginal stability. For realizable feedback gain factors, this feedback system can suppress the kink mode amplitude for times that are very long compared with the L/R time-scale of the passive shell system. The circuit equation approach discussed provides a useful means for comparing various control strategies for $n \geq 1$ kink mode control, and allows useful analogies to be drawn between kink mode control and the control of $n = 0$ vertical position instabilities.

1. INTRODUCTION

The ability to control the $n = 0$ vertical position instability in tokamaks with a shaped cross-section has been crucial to the success of modern tokamak fusion research [1–8]. The key to the success of vertical position control is the integration of a passive stabilizing system that slows the vertical growth rate from an ideal time-scale (\sim microseconds) to a resistive wall time-scale (\sim milliseconds), and an active feedback system which controls the measured amplitude of the instability.

With the high temperature regimes achievable, current large scale tokamak programmes are now tackling the significant challenge of sustaining high- β plasmas near the ideal MHD β limit for times long compared with the energy confinement time, τ_E . Major disruptions often prematurely terminate high- β plasma discharges [9]. The ideal MHD mode most often suspected of inducing high- β disruptions is the pressure driven external kink. Several experimental results indicate that a passive shell (either a close fitting vacuum vessel wall or passive conducting plates) can reduce the external kink growth rates to the resistive time-scale of the passive shell system [10, 11]. The resulting resistive wall mode (RWM) [12] can

then, in principle, be controlled by a combination of the passive shell system and an active feedback control system that operates on a modest time-scale in a manner similar to what has been successful for $n = 0$ vertical position control.

Recently, various schemes for controlling the resistive wall mode have been proposed which utilize integration of both active (feedback controlled) and passive stabilizing systems. The ‘intelligent shell’ scheme was originally developed by Bishop [13] and proposed as a method to control locked modes in RFP devices. The method reproduces the magnetic effects of a virtual perfectly conducting wall, freezing the perturbed magnetic flux on a toroidal surface at some appropriate distance from the plasma. The fake rotating shell (FRS) scheme was developed by Fitzpatrick and Jensen [14, 15] and proposed as an efficient means for stabilizing resistive wall modes on tokamaks. Here a network of feedback controlled conductors surrounds the plasma and passive shell and can be made to act like a secondary rotating shell. The combination of a stationary conducting shell and a rotating secondary shell was shown by Gimblett [16] to be capable of completely stabilizing resistive wall modes.

Here, we present a formulation for resistive wall mode feedback control utilizing concepts from

electrical circuit theory. We consider the perturbed plasma current, the poloidal passive shell and the active control coil as lumped parameter electrical circuits obeying the usual laws of linear circuit theory (Kirchoff's voltage and current laws). An inductance matrix describes the interactions between the coupled circuits and is useful for evaluating the merits of proposed designs. The off-diagonal terms (mutual inductances) are directly related to the geometry of the coupled components. A simple set of coupled linear differential equations describe the time evolution of the circuit currents. They have a form familiar to both physicists and engineers and facilitate the analysis necessary for system design. This approach has proved useful for both the analysis and the design of power and control systems for vertical position control [4].

In Sections 2 and 3, we derive circuit equations which describe the interaction of a kink-unstable plasma with a resistive wall and with active feedback coils. The derivation assumes a circular cylindrical pinch for the plasma, and makes use of the thin shell approximation for the resistive wall. In contrast to the usual treatment of kink modes (e.g., see Ref. [12]) our formulation separates the vacuum helical flux into contributions corresponding to isolated currents in the various conducting structures (Fig. 1). A mutual inductance matrix describes the coupling between the elements. In Sections 4 and 5 we discuss the dispersion relation obtained from the circuit equations without active feedback. We show that the roots of the dispersion relation reproduce known solutions for the growth rate of kink modes. An 'effective self-inductance' of the plasma is introduced which describes the strength of the unstable plasma kink drive. This inductance embodies all of the relevant MHD properties of the plasma. Finally, the resistive wall mode limit of the full circuit equations, including feedback, is taken and analogies to the circuit equations for the $n = 0$ vertical instability are drawn.

In Section 6 we examine the dispersion relation for the RWM circuit equations using different models for the feedback. The feedback coil is driven by a voltage which is proportional to a linear combination of the three independent circuit currents; the perturbed plasma current, I_1 , the passive shell current, I_2 , and the active coil current, I_3 . We neglect consideration of derivative and integral control terms in the feedback law in order to simplify the comparison between various feedback schemes. These additional terms are sometimes used to improve the transient or steady state characteristics, but it is desirable that

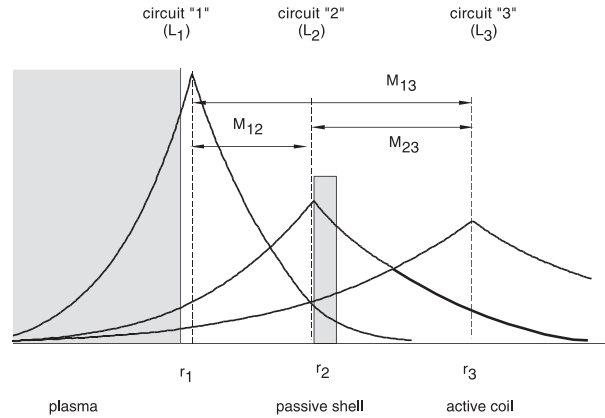


FIG. 1. A plasma extends from $r = 0$ to $r = r_1$. A (magnetically) thin passive conducting shell, of thickness δ , is located at $r = r_2$. An active feedback coil is at radius r_3 . The perturbed plasma current is represented as a current in an electrical circuit, labelled '1' at radius r_1 . The eddy current on the passive shell is a current in circuit '2' at radius r_2 , and the active feedback current is a current in circuit '3' at radius r_3 . L_i is the self-inductance of circuit 'i', and the M_{ij} are mutual inductances between circuits 'i' and 'j', which relate the current in circuit 'j' to the flux at r_i . Helical flux contributions from the individual circuit currents are shown.

they be corrections to a basically stable system. Four feedback schemes are discussed: the explicit displacement (ED), shell current (SC), total flux (TF) and FRS schemes. In the explicit displacement scheme the sensor signal is the perturbed plasma current, I_1 . The control scheme is analogous to feedback control on $\delta z I_{\text{plasma}}$ for $n = 0$ vertical displacement instabilities, where δz is the measured displacement of the equilibrium plasma. Although direct measurement of I_1 is probably not practical for $n \geq 1$ kink mode control because of the difficulty in accurately distinguishing this plasma perturbation from contributions due to the eddy currents in the passive shell, a discussion of this scheme provides a useful means for comparing the relative merits of other schemes and for comparing these schemes with known features of $n = 0$ control. In the SC scheme, which is equivalent to Bishop's intelligent shell scheme [13], the sensor signal is the shell eddy current, I_2 , representing the flux loss due to the finite resistivity of the shell. This scheme has been implemented successfully for $n = 0$ vertical position control in PBX-M [8] and is shown here to be an attractive scheme for $n = 1$ kink mode control. In the TF and FRS schemes the sensor signal is the total perturbed flux, which depends on I_1 , I_2 and I_3 . In the TF scheme the voltage applied to the feedback coil is

proportional to the measured flux, with a constant of proportionality (the gain) that is real. In the FRS scheme, however, the gain coefficient is purely imaginary. This introduces a phase shift between the sensor loop and the feedback coil and leads to a feedback field that rotates relative to the plasma perturbation. The mechanism of FRS scheme stabilization is therefore analogous to kink mode stabilization by plasma rotation, a subject of active study in recent years by several authors [17–20]. The feedback schemes are compared using a variety of techniques from control engineering. We end with a summary and conclusions.

The work described in this article is an extension of research presented by the authors in Refs [21, 22]. A related approach can be found in Ref. [23].

2. DERIVATION OF THE PLASMA CIRCUIT EQUATION

We begin with the familiar eigenmode equations [24] used to determine the stability of a large aspect ratio tokamak with low β ($\sim \epsilon^2$, where ϵ is the inverse of the aspect ratio):

$$\frac{d}{dr} \left((\gamma^2 \tau_A^2 + \hat{F}^2) r \frac{d}{dr} (r \xi_r) \right) - \left(m^2 (\gamma^2 \tau_A^2 + \hat{F}^2) + r \frac{d\hat{F}^2}{dr} \right) \xi_r = 0. \quad (1)$$

The form of (1) corresponds to that of Wesson [25], and assumes incompressibility. In Eq. (1), ξ_r is the radial component of the fluid displacement,

$$\hat{F} = [a/B_\theta^0(a)][B_\theta^0(r)/r][(m - nq(r))]$$

determines the equilibrium current profile ($q = rB_z/RB_\theta^0$ is the equilibrium safety factor), m and n are poloidal and toroidal mode numbers, γ is the growth rate of the mode (which may be complex) and $\tau_A = \rho_0^{1/2} a/B_\theta^0(a)$ is the edge poloidal Alfvén time. Equation (1) is solved subject to a regularity condition for ξ_r at the magnetic axis, $r = 0$, and a plasma–vacuum boundary condition at the plasma edge, $r = a$, of the form

$$\frac{1}{\xi_r} \frac{d(r\xi_r)}{dr} \Big|_{r=a} = \frac{mf^2}{\gamma^2 \tau_A^2 + f^2} \left(\frac{a\psi'(a_+)}{m\psi(a_+)} + \frac{2}{f} \right) \quad (2)$$

where

$$f = m - nq_a \quad (3)$$

and $\psi(a_+)$ is the vacuum poloidal flux evaluated at the unperturbed plasma surface. The flux is defined in terms of the vacuum magnetic field by

$$\mathbf{B} = \nabla \times \frac{\psi}{2\pi R_0} \hat{z} \quad (4)$$

and ψ' denotes the derivative of the flux with respect to r .

The boundary condition, Eq. (2), is used to provide a circuit equation for the plasma, as follows: define the quantity β^0 such that

$$\frac{1}{\xi_r} \frac{d(r\xi_r)}{dr} \Big|_{r=a} \equiv m\beta^0. \quad (5)$$

Then Eq. (2) can be rewritten as

$$(\gamma^2 \tau_A^2 + f^2) \beta^0 = f^2 \frac{a\psi'(a_+)}{m\psi(a_+)} + 2f. \quad (6)$$

We suppose that the plasma is surrounded by a resistive wall and by active feedback coils. Using a terminology consistent with electrical networks, we denote the current carrying ‘circuit’ corresponding to the perturbed plasma as circuit ‘1’, the circuit corresponding to the resistive wall as ‘2’ and the circuit corresponding to the active feedback coils as ‘3’ (Fig. 1). Now write the poloidal flux in the vacuum region at the unperturbed plasma boundary in terms of inductive contributions from the individual circuits,

$$\psi(a_+) = L_1 I_1 + M_{12} I_2 + M_{13} I_3. \quad (7)$$

L_1 is the self-inductance of the plasma circuit, and the M_{1j} are mutual inductances between the plasma and the resistive wall, and the plasma and active coils. Similarly, for the radial derivative of the poloidal flux,

$$\psi'(a_+) = L'_1 I_1 + M'_{12} I_2 + M'_{13} I_3. \quad (8)$$

Using (7) and (8), Eq. (6) can be rewritten as

$$\begin{aligned} & \left((\gamma^2 \tau_A^2 + f^2) \beta^0 - f^2 \frac{a}{m} \frac{L'_1}{L_1} - 2f \right) L_1 I_1 \\ & + \left((\gamma^2 \tau_A^2 + f^2) \beta^0 - f^2 \frac{a}{m} \frac{M'_{12}}{M_{12}} - 2f \right) M_{12} I_2 \\ & + \left((\gamma^2 \tau_A^2 + f^2) \beta^0 - f^2 \frac{a}{m} \frac{M'_{13}}{M_{13}} - 2f \right) M_{13} I_3 = 0. \end{aligned} \quad (9)$$

This circuit equation for the plasma can be further simplified using the relations $aL'_1/mL_1 = -1$, $aM'_{1j}/mM_{1j} = +1$, which are valid in the cylindrical limit (Appendix A).

In the usual treatment of kink mode stability, β^0 would be determined from the self-consistent solution of Eqs (1) and (2). Clearly, its value depends on the calculated growth rate. However, for a fixed position of the conducting wall the growth rate is

uniquely determined by the equilibrium current profile. In Eq. (9), it is therefore possible to interpret β^0 as an equilibrium parameter, the value of which specifies the equilibrium plasma current profile. The special case of a plasma with a uniform current density profile ($\hat{F} = \text{const}$) provides a useful example. Equations (1), (2) and (5) are trivially solved to yield $r\xi_r \sim r^m$, and $\beta^0 = 1.0$, independent of the location of the conducting wall. For more general profiles the value of β^0 can differ substantially from unity (Section 4, Fig. 2).

3. CIRCUIT EQUATIONS FOR THE RESISTIVE WALL AND ACTIVE FEEDBACK SYSTEM

To derive an equation for the circuit corresponding to the resistive wall (circuit 2), we start with

$$\frac{\partial\psi(r_w)}{\partial t} = L_2 \frac{\partial I_2}{\partial t} + M_{21} \frac{\partial I_1}{\partial t} + M_{23} \frac{\partial I_3}{\partial t} \quad (10)$$

which is obtained by taking the time derivative of the perturbed flux at the resistive wall utilizing (7). The radial component of Faraday's law provides an equation which replaces the LHS of (10): the r component of Faraday's law is

$$\partial B_r / \partial t = -\frac{im}{r} E_z. \quad (11)$$

Here, we have made the thin wall approximation so that only the axial component of the electric field, E_z , is retained. Equation (4) relates B_r to ψ , and Ohm's law, $E_z = \eta J_z$, provides an equation for E_z in terms of the wall resistivity, η , and the wall eddy current density, J_z . Finally, each side of (11) is integrated across the wall (of thickness δ) to obtain

$$\partial\psi(r_w)/\partial t = -R_2 I_2 \quad (12)$$

where

$$I_2 = \frac{2\pi r_w}{2m} \int_{r_w}^{r_w+\delta} J_z dr \quad (13)$$

is the current in the resistive wall circuit, and

$$R_2 = \frac{2m\eta R_0}{r_w \delta} \quad (14)$$

is the circuit resistance. The full circuit equation describing the interaction of the resistive wall with the plasma and active feedback circuits is obtained by replacing the LHS of Eq. (10) by the RHS of Eq. (12) and taking the Laplace transform of the result, thus

$$(\gamma L_2 + R_2)I_2 + \gamma M_{21}I_1 + \gamma M_{23}I_3 = 0. \quad (15)$$

The circuit equation for the active feedback coils is derived similarly. The only difference is the inclusion of a voltage term to drive the feedback circuit, thus

$$\gamma M_{31}I_1 + \gamma M_{32}I_2 + (\gamma L_3 + R_3)I_3 = V_3. \quad (16)$$

The form of the feedback voltage, V_3 , depends on the details of the feedback control scheme and will be discussed later.

Equations (9), (15) and (16) are circuit equations for the perturbed plasma current, resistive wall and active feedback circuits, respectively. We will build towards a discussion of the full dispersion relation for the Laplace transform variable γ , by first considering some special cases.

4. CIRCUIT DISPERSION RELATION (CDR) FOR PLASMA WITH NO PASSIVE OR ACTIVE FEEDBACK

Consider an isolated plasma with no resistive wall (namely, with the wall at infinity) and no active feedback system. A dispersion relation is obtained from Eq. (9) by equating the coefficient of $L_1 I_1$ to zero. Thus,

$$\gamma^2 \tau_A^2 = \frac{2f}{\beta^0} \left(1 - f \frac{(\beta^0 + 1)}{2} \right) \equiv \gamma_\infty^2 \tau_A^2. \quad (17)$$

For a constant current density profile, where $\beta^0 = 1$, the familiar form for the dispersion relation of ideal external kinks is obtained, namely $\gamma_\infty^2 \tau_A^2 = 2f(1-f)$. The kink is unstable for f values in the range $0 < f < 1$. For a more general current profile, $\gamma_\infty^2 \tau_A^2$ can be determined numerically by solving Eqs (1) and (2). For example, consider a current profile of the 'Wesson' form [25]

$$J_z = J(0) \left(1 - \frac{r^2}{a^2} \right)^{q_a/q_0-1} \quad (18)$$

where q_a/q_0 is the ratio of the safety factor at the edge of the plasma to the corresponding value at the magnetic axis. The value of q_a/q_0 determines the peakedness of the current profile. The Wesson profile is consistent with a safety factor profile of the form

$$q(r) = q_a \frac{r^2/a^2}{1 - (1 - r^2/a^2)^{q_a/q_0}}. \quad (19)$$

Assuming an axis safety factor value of $q_0 = 0.8$, an $m = 2, n = 1$ kink external mode is found to be unstable for edge safety factor values in the range $1.32 < q_a < 2.0$, corresponding to f values in the

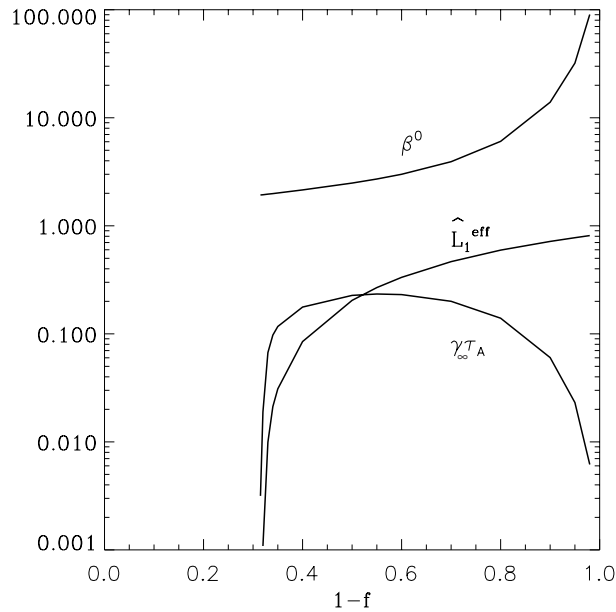


FIG. 2. For a Wesson current profile (Eq. (18)) with axis safety factor $q_0 = 0.8$, unstable to an $m = 2$, $n = 1$ external kink instability, the profile parameter β^0 (Eq. (5)), growth rate $\gamma_\infty \tau_A$ (Eq. (17)) and plasma effective self-inductance \hat{L}_1^{eff} (Eq. (21)) are plotted as functions of $1-f$, where $f = m - nq_a$.

range $0.68 > f > 0.0$. For this range of profile shapes, β^0 varies between 1.9 and ∞ , as shown in Fig. 2. The dependence of $\gamma_\infty \tau_A$ on f is also shown in the figure.

In the remainder of this article we assume $\gamma_\infty^2 \tau_A^2 > 0$, corresponding to plasma conditions (values of f and β^0) such that, without feedback, the plasma is unstable to an external kink mode.

5. CDR FOR PLASMA WITH CONDUCTING WALL AND NO ACTIVE FEEDBACK

Consider now the effect of a conducting wall placed at a finite radius $r = r_2$. We assume that the conducting wall has been sensibly placed so that the wall radius lies within the critical radius for which ideal external kinks are stabilized by a perfectly conducting wall for some desired operating range of plasma profiles (values of f and β^0 in our model). This restriction on r_2 provides a constraint on the mutual inductance M_{12} . The constraint is obtained by setting $R_2 = 0$ in Eq. (15), suppressing the terms involving the circuit label ‘3’ in Eqs (9) and (15), solving for

$\gamma^2 \tau_A^2$, and forcing the stability condition $\gamma^2 \tau_A^2 < 0$. The result is

$$L_1^{\text{eff}} - \frac{M_{12}^2}{L_2} < 0. \quad (20)$$

Here, an ‘effective’ self-inductance for the plasma circuit has been defined as

$$L_1^{\text{eff}} \equiv L_1 \left(\frac{\gamma_\infty^2 \tau_A^2}{\gamma_\infty^2 \tau_A^2 + \frac{2f^2}{\beta^0}} \right) = L_1 \left(\frac{1 - f(\beta^0 + 1)/2}{1 - f(\beta^0 - 1)/2} \right). \quad (21)$$

L_1^{eff} is the drive term for the $n \geq 1$ MHD instability. For a constant current density profile with $\beta^0 = 1.0$, $L_1^{\text{eff}} = L_1(1 - f)$. For a more general current profile such as the Wesson profile, the evaluation of L_1^{eff} requires, first, the calculation of β^0 by numerical integration of Eqs (1), (2) and (5), then substitution of β^0 into Eq. (21). Fixing $q_0 = 0.8$ leads to the dependence of L_1^{eff} on f shown in Fig. 2. The value of L_1^{eff}/L_1 is always less than unity, independently of the choice of current profile.

Equation (20) is a design criterion for the passive shell system. For control of $n \geq 1$ kink modes, this condition must be satisfied, independently of any details of the active feedback system. If the plasma drive is fixed, Eq. (20) defines a maximum radius at which an ideal passive shell can be placed to stabilize the kink mode. If, instead, the ideal shell location is fixed, Eq. (20) defines a maximum plasma drive which can be stabilized by the shell. For example, a plasma with an ideal conducting wall at $r_2/r_1 = 1.2$ is stable to $m = 2$, $n = 1$ kink modes for $\beta^0 = 1.0$ and f in the range $0.518 < f < 1$.

Equation (20) is analogous to the equivalent condition for $n = 0$ control,

$$M_{\text{ext}}'' - \frac{M_{12}^{\prime 2}}{L_2} < 0. \quad (22)$$

The two conditions (Eqs (20) and (22)) are prerequisites for feedback stabilization of the respective modes. For the $n \geq 1$ instability, the condition can be interpreted as follows: a helical plasma current perturbation I_1 gives rise to a flux change of $I_1 M_{12}$ at the ideal passive shell. This flux change induces a current on the shell of magnitude $I_2 = I_1 M_{12}/L_2$. The induced current in turn produces a flux change of $I_2 M_{21}$ at the plasma surface. For the ideal passive shell to stabilize the kink mode, this flux change must be greater than the flux change $L_1^{\text{eff}} I_1$ associated with the plasma instability. For the $n = 0$ vertical instability the energy source for the instability

is the external field curvature, M''_{ext} , instead of L_1^{eff} . The flux change is due to the vertical displacement of the equilibrium plasma column so that a spatial derivative of the mutual inductance, M'_{12} , appears in Eq. (22) instead of M_{12} .

Assuming a resistive wall location such that Eq. (20) is satisfied, the growth rate for the kink mode is reduced to the time-scale of the resistive shell. Then $\gamma\tau_A \ll \gamma\tau_2 \sim 1$. The kink mode is now called an RWM. The RWM limit for the circuit equations is obtained by dropping the $\gamma^2\tau_A^2$ terms in Eq. (9). The plasma circuit equation becomes a constraint condition

$$L_1^{\text{eff}}I_1 + M_{12}I_2 + M_{13}I_3 = 0. \quad (23)$$

We can also rewrite Eqs (15) and (16), non-dimensionalizing the growth rate γ using the L/R time constants of the resistive wall and feedback coil systems,

$$(\gamma\tau_2)M_{21}I_1 + (\gamma\tau_2 + 1)L_2I_2 + (\gamma\tau_2)M_{23}I_3 = 0 \quad (24)$$

and

$$(\gamma\tau_3)M_{31}I_1 + (\gamma\tau_3)M_{32}I_2 + (\gamma\tau_3 + 1)L_3I_3 = V_3\tau_3. \quad (25)$$

Here, $\tau_2 = L_2/R_2$ and $\tau_3 = L_3/R_3$. Equations (23), (24) and (25) are circuit equations describing the interaction of a feedback circuit with an RWM.

The dispersion relation for an RWM with no feedback coil is obtained by solving Eqs (23) and (24), dropping terms having the subscript '3'. We obtain

$$\gamma\tau_2 = \frac{-1}{1 - \frac{\hat{M}_{12}\hat{M}_{21}}{\hat{L}_1^{\text{eff}}}} \equiv \Gamma\tau_2 \quad (26)$$

where

$$\hat{L}_1^{\text{eff}} \equiv \frac{L_1^{\text{eff}}}{L_1}, \quad \hat{M}_{ij} \equiv \frac{M_{ij}}{L_i} \quad (27)$$

are normalized self-inductances (effective) and mutual inductances.

Assuming a flat current density for the plasma, and cylindrical limit expressions for the mutual inductances, it follows that $\beta^0 = 1$, $\hat{L}_1^{\text{eff}} = (1 - f)$, and $\hat{M}_{12} = \hat{M}_{21} = (a/r_2)^m$. The growth rate, Eq. (26), simplifies to

$$\gamma\tau_2 = -\frac{1}{1 - \frac{M_{12}^2}{L_2L_1^{\text{eff}}}} = -\frac{1}{1 - \frac{(a/r_2)^{2m}}{(1-f)}}. \quad (28)$$

The expression on the RHS of the second equality is the familiar growth rate for the RWM. However, it is interesting to compare the first equality in the dispersion relation, expressed in terms of inductances, with the dispersion relation for the vertical position instability of a filamentary plasma, namely

$$\gamma\tau_2^{n=0} = -\frac{1}{1 - \frac{M_{12}^2}{L_2M''_{\text{ext}}}}. \quad (29)$$

L_1^{eff} represents the energy source term for the $n \geq 1$ MHD instability, analogous to M''_{ext} for the $n = 0$ vertical positional instability.

6. CDR FOR PLASMAS WITH VARIOUS ACTIVE FEEDBACK SCHEMES

We now examine the dispersion relation obtained using different models for the feedback. The various schemes differ in the choice of sensor signal. The signal is determined by some combination of the three independent circuit currents: the perturbed plasma current I_1 , the passive shell current I_2 and the active coil current I_3 . Four feedback schemes are discussed: the ED, SC, TF and FRS schemes.

6.1. Explicit displacement feedback

The first feedback scheme we consider assumes that the voltage supplied to the feedback circuit is proportional to the perturbed plasma current flowing in the plasma circuit, I_1 . For the voltage appearing on the RHS of Eq. (25) we write

$$V_3\tau_3 = G_e L_1 I_1 \quad (30)$$

where G_e is the (real) voltage gain. We discuss this case because of its close analogy with $n = 0$ feedback schemes where an array of flux loop sensors are used to infer the vertical displacement δz of the plasma from its equilibrium location. Feedback on I_1 is equivalent to feedback on $I_{\text{plasma}}\delta z$ for the $n = 0$ mode. Such a feedback scheme has been implemented for $n = 0$ control in most shaped tokamak experiments [1–8]. Although direct measurement of I_1 is probably not practical for $n \geq 1$ kink mode control because of the difficulty in accurately distinguishing this plasma perturbation from contributions due the eddy currents in the passive shell, a discussion of this scheme provides a useful means for comparing the relative merits of the SC, TF and FRS feedback schemes and for comparing these schemes with known features of $n = 0$ control.

Using Eq. (30) on the RHS of Eq. (25) and solving Eqs (23)–(25), a quadratic formula for the growth rate is easily obtained (Appendix B). If we assume that the L/R time of the active circuit is short compared with the L/R time of the passive conducting shell, $\tau_3 \ll \tau_2$, the dominant root of the dispersion relation is

$$\gamma\tau_2 \approx \frac{1 + G_e \frac{\hat{M}_{31}}{\hat{L}_1^{\text{eff}}}}{\frac{1}{\Gamma\tau_2} - G_e \left(\hat{M}_{31} - \hat{M}_{32}\hat{M}_{21} \right) \frac{1}{\hat{L}_1^{\text{eff}}}}. \quad (31)$$

Here $\Gamma\tau_2 > 0$ is the growth rate of the RWM in the absence of active feedback and was first defined in Eq. (26). If $G_e < 0$, the growth rate decreases with increasing magnitude of the voltage gain. Complete stabilization is achieved when $G_e < -\hat{L}_1^{\text{eff}}/\hat{M}_{31}$.

The term

$$\begin{aligned} G_e \left(\hat{M}_{31} - \hat{M}_{32}\hat{M}_{21} \right) \frac{1}{\hat{L}_1^{\text{eff}}} \\ = \frac{G_e}{L_3} \left(M_{31} - \frac{M_{32}M_{21}}{L_2} \right) \frac{1}{L_1^{\text{eff}}} \end{aligned}$$

appearing in the denominator of Eq. (31) is a measure of the shielding of the field from the active coil by the conducting shell. When the active coil is energized with current I_3 , an eddy current is generated on the passive shell of magnitude $I_2 = I_3 M_{32}/L_2$. This current produces a helical magnetic flux $\psi = (I_3 M_{32}/L_2) M_{21}$ on the plasma surface in opposition to the stabilizing direct flux $M_{31} I_3$ from the active coil. If M_{31} is comparable to $M_{32} M_{21}/L_2$ the active control field is shielded from the plasma and the voltage required to decrease the growth rate to a desired level is increased. The plasma drive term, L_1^{eff} , affects the overall gain magnitude but does not affect the shielding balance.

In the limit of infinite aspect ratio and radial symmetry, $\hat{M}_{32}\hat{M}_{21} := (r_2/r_3)^m (r_1/r_2)^m = (r_1/r_3)^m = \hat{M}_{31}$, and the shielding factor $\hat{M}_{31} - \hat{M}_{32}\hat{M}_{21}$ is zero (corresponding to perfect shielding). At finite aspect ratio (or if the aspect ratio is infinite and the circuit elements do not have radial symmetry) this term will be non-zero and the shielding is imperfect. To assess the impact of finite shielding we define

$$\Delta = \frac{\hat{M}_{31} - \hat{M}_{32}\hat{M}_{21}}{\hat{M}_{31}} \quad (32)$$

and eliminate any occurrence of $\hat{M}_{31} - \hat{M}_{32}\hat{M}_{21}$ in the circuit dispersion relations in favour of Δ . Results will

be presented for $\Delta = 0.0$ (the cylindrical limit), and for $\Delta = 0.2$. We assume this finite value of Δ is a ‘typical’ value. To justify such a value we have calculated numerically the mutual and self-inductances of $m = 3$, $n = 1$ helical wire filaments wound on nested toroidal surfaces. The major radius of each torus is $R = 3.0$ m. The aspect ratio of the inner torus (representing the plasma surface) is $R/r_1 = 4.5$, and the minor radii of the toroidal surfaces on which filaments representing the passive shell and the active coil are wound are expressed by the ratios $r_2/r_1 = 1.2$, $r_3/r_1 = 1.3$. Assuming a 1.0 cm cross-section for calculating the self-inductance of the wire corresponding to the passive shell, the calculated value of Δ is 0.24. A more detailed calculation of the shielding factor only makes sense, in our view, if the circuit equation approach presented in this article is generalized to include the effects of multiple helicities at finite aspect ratio. This is beyond the scope of the present work.

The validity of the assumption $\tau_3 \ll \tau_2$ which led to Eq. (31) depends on the details of the control system design. For example, the $n = 0$ feedback control systems on Alcator C-Mod [26], PBX-M [8] and DIII-D [27] have active/passive time constant ratios of 0.6, 1.0 and 2.6, respectively. To examine the behaviour of the feedback system for general values of τ_3/τ_2 it is convenient to trace numerically the loci of roots of the dispersion relation as the gain, G_e , is varied. Figure 3 presents root locus plots [28] for the ED scheme. The plasma parameters are $f = 0.6$ and $\beta^0 = 1.0$; the passive shell and feedback coil radii are $r_2/r_1 = 1.20$ and $r_3/r_1 = 1.30$, respectively. In Figs 3(a,b) the ratio of time constants of the active coil and the passive shell is $\tau_3/\tau_2 = 5.0$. Root loci are shown for $\Delta = 0.0$ and $\Delta = 0.2$. Without feedback ($G_e = 0$) both roots of the dispersion relation are real and have opposite sign (one stable and one unstable). As the gain is increased, the unstable root moves towards the stable region ($\text{Re}(\gamma) < 0$). If the shielding factor, Δ , is zero (Fig. 3(a)) there is no value of the gain for which stability is achieved. Beyond some value of $|G_e^{\text{crit}}|$ the growth rate becomes complex ($\text{Im}(\gamma) \neq 0$); the oscillation frequency increases rapidly with increasing gain magnitude. For finite values of Δ the system growth rate is damped (Fig. 3(b)). However, the oscillation frequency can dominate the damping rate, and the feedback system is ineffective. The system characteristics improve with increasing gain. With large enough gain magnitude, the oscillation frequency becomes zero.

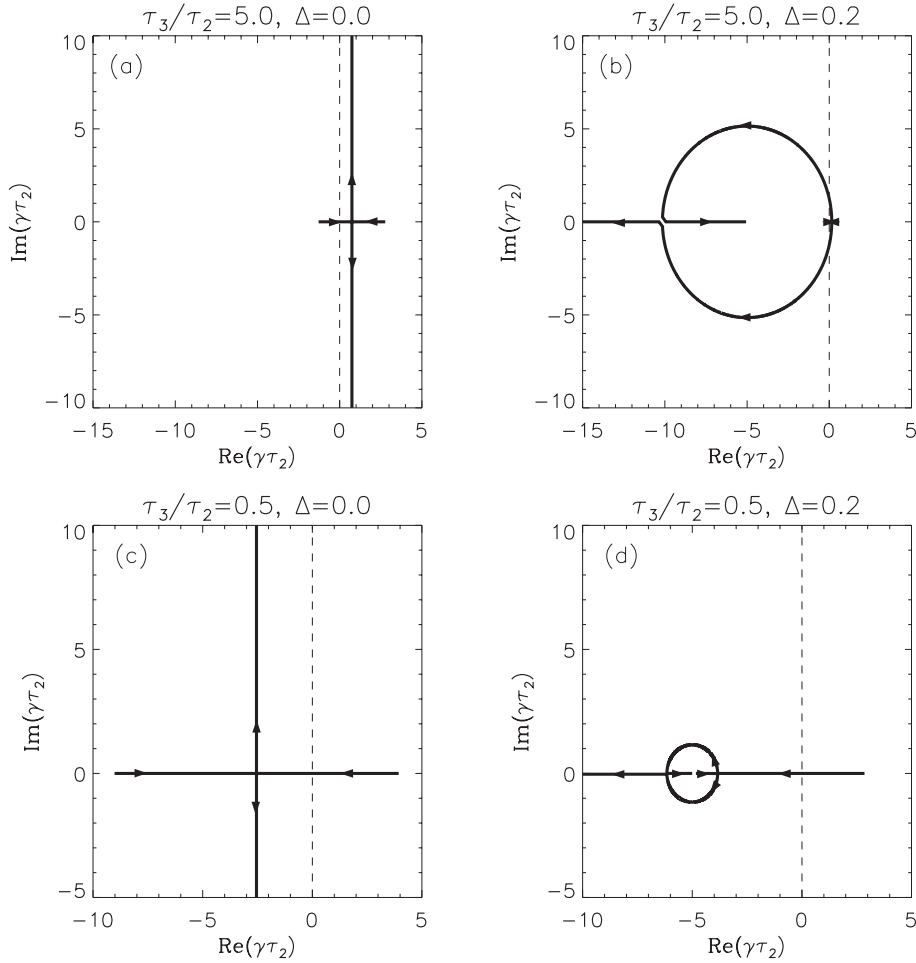


FIG. 3. Root locus plots for the ED feedback scheme, Section 6.1. The loci of roots of the dispersion relation (Eq. (68)) are traced as the gain, $G_e < 0$, is varied. For each of two values of the ratio of time constants for the active and passive feedback systems, τ_3/τ_2 , two values of the shielding factor, $\Delta = (\hat{M}_{31} - \hat{M}_{32}\hat{M}_{21})/\hat{M}_{31}$, are assumed: (a) $\tau_3/\tau_2 = 5.0$, $\Delta = 0.0$, (b) $\tau_3/\tau_2 = 5.0$, $\Delta = 0.2$, (c) $\tau_3/\tau_2 = 0.5$, $\Delta = 0.0$, (d) $\tau_3/\tau_2 = 0.5$, $\Delta = 0.2$. The resistive wall and active feedback circuits are located at $r_2/r_1 = 1.20$, $r_3/r_1 = 1.30$, respectively. The plasma parameters are $f = 0.6$, $\beta^0 = 1.0$. The arrows denote the direction of motion of the roots as the magnitude of the gain is increased.

Figures 3(c) and (d) show root locus plots for $\tau_3/\tau_2 = 0.5$ with plasma parameters $\beta^0 = 1.0$, $f = 0.6$. For this smaller value of $\tau_3/\tau_2 = 0.5$ (compared with that of Figs 3(a) and (b)), the unstable root can be stabilized without oscillation. Clearly, it is desirable to have feedback system parameters such that the damping is large and purely real. At some critical gain value the damping rate becomes complex. Figure 4 shows a plot of the maximum purely real damping rate as a function of τ_3/τ_2 . We see that if the damping rate is required to be non-oscillatory there is a design requirement on τ_3/τ_2 for a given wall

and active coil position. If the required damping rate using ED feedback is at least one inverse wall time constant then $\tau_3/\tau_2 \lesssim 1$ is required.

6.2. Shell current feedback

The second feedback scheme we consider assumes that the voltage supplied to the feedback circuit is proportional to the measured eddy current in the resistive shell. Specifically, for the voltage appearing on the RHS of Eq. (25) we write

$$V_3\tau_3 = G_s L_2 I_2 \quad (33)$$

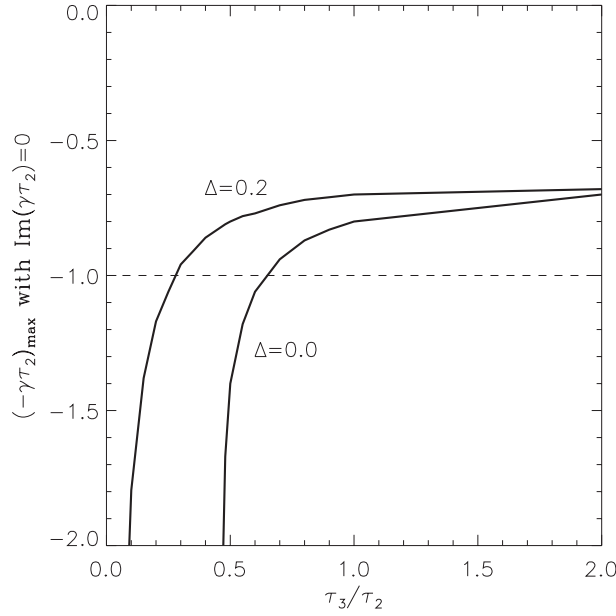


FIG. 4. Maximum value of the mode damping rate, $\text{Re}(\gamma\tau_2)$, in the ED scheme for which the oscillation frequency, $\text{Im}(\gamma\tau_2)$, remains zero. Large values of $|\text{Re}(\gamma\tau_2)|$ are desirable. This favours small τ_3/τ_2 .

where G_s is the (real) feedback gain. Assuming $\tau_3 \ll \tau_2$, the dominant root of the quadratic dispersion relation (Appendix B) is found to be

$$\gamma\tau_2 \approx \frac{1}{\frac{1}{\Gamma\tau_2} - G_s \left(\hat{M}_{32} - \frac{\hat{M}_{31}\hat{M}_{12}}{\hat{L}_1^{\text{eff}}} \right)}. \quad (34)$$

A necessary condition for decreasing the growth rate by increasing the voltage in the feedback circuit is

$$G_s \left(\hat{M}_{32} - \frac{\hat{M}_{31}\hat{M}_{12}}{\hat{L}_1^{\text{eff}}} \right) < 0. \quad (35)$$

The LHS of Eq. (35) exhibits the shielding effect of the passive shell. In contrast with the ED scheme, where the shielding depended on purely geometric factors, the magnetic shielding in SC feedback includes the plasma effective inductance L_1^{eff} . Here, the active coil produces the flux $\psi = I_3 M_{31}$ at the plasma surface, which drives a circuit current $I_1 = I_3 M_{31} / L_1^{\text{eff}}$. This, in turn, creates a flux $\psi = I_3 M_{31} M_{12} / L_1^{\text{eff}}$ at the passive shell. To produce a stabilizing effect, this flux should be larger than the direct flux at the shell due to the control field, $I_3 M_{32}$.

Figure 5 shows a root locus plot for feedback control using the SC feedback scheme. The plasma parameters are $\beta^0 = 1$, $f = 0.6$; the passive shell and active coil radii are $r_2/r_1 = 1.20$ and $r_3/r_1 = 1.30$, respectively. For comparison with the ED root locus plots, shielding parameter values of $\Delta = 0.0$ and 0.2 are considered for time constant ratios of the active and passive systems of $\tau_3/\tau_2 = 5.0$ and 0.5 . The sign of the gain is chosen so that with increasing gain the roots both move in the direction of increased stability ($G_s > 0$). As noted in Appendix B, both roots of the dispersion relation are purely real for all assumed values of τ_3/τ_2 and of the gain, G_s . The unstable root approaches zero as the stable root approaches negative infinity. The absence of oscillation is in contrast to the ED scheme discussed in the previous section, and to the TF and FRS schemes to be discussed later. Complete stabilization of the $n \geq 1$ mode is not possible. However, with a large enough gain the growth rate can be made as small as desired. In Section 8, we will see that the stable root determines the system response time, and the fact that this root rapidly obtains large negative values as the gain is increased makes the SC feedback method an attractive feedback scheme in spite of the fact that there is always one unstable root. The dependence of growth rate on the plasma drive parameter, f , will be discussed in Section 9. The feasibility of SC feedback has been demonstrated for $n = 0$ position control in PBX-M by routinely producing strongly shaped plasmas, applying feedback on the $n = 0$ component of the eddy current on the shell [8]. The sensor signal was obtained from Rogowski coils inserted in the passive shell. Some advantages of SC feedback for $n = 0$ mode control compared with ED feedback have been reported in Ref. [8].

6.3. Total flux feedback

For this feedback scheme the voltage is assumed to act in response to a measurement of the total perturbed flux at radius $r = r_0$. The voltage appearing in Eq. (25) is written as

$$V_3\tau_3 = G_t(M_{10}I_1 + M_{20}I_2 + M_{30}I_3) \quad (36)$$

and we assume that the gain, G_t , is real. A dispersion relation is found for the growth rate in a manner analogous to that discussed in the previous two sections.

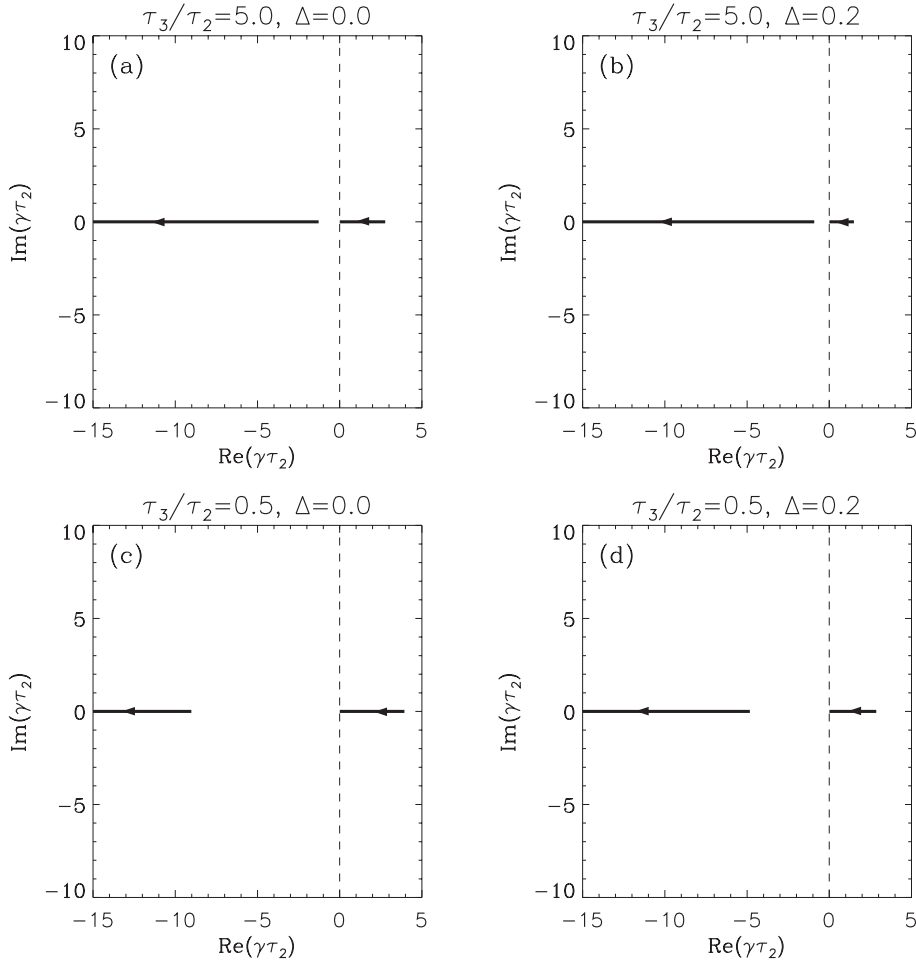


FIG. 5. Root locus plots for the SC feedback scheme, Section 6.2. The plasma parameters and feedback circuits are the same as in Fig. 3. The gain, G_s , is chosen positive for this scheme. As G_s is increased, the unstable root approaches the origin, the stable root approaches negative infinity. Both roots are real for all values of τ_3/τ_2 and Δ .

If $\tau_3 \ll \tau_2$ the solution corresponding to the dominant root is (Appendix B)

$$\gamma\tau_2 \approx \frac{1 - G_t \left(\hat{M}_{30} - \frac{\hat{M}_{31}\hat{M}_{10}}{\hat{L}_1^{\text{eff}}} \right)}{\frac{1}{\Gamma\tau_2} - G_t \mathcal{A}}$$

where

$$\begin{aligned} \mathcal{A} = & \frac{\hat{M}_{30}}{\Gamma\tau_2} + \hat{M}_{20} \left(\hat{M}_{32} - \frac{\hat{M}_{31}\hat{M}_{12}}{\hat{L}_1^{\text{eff}}} \right) \\ & + (\hat{M}_{31} - \hat{M}_{32}\hat{M}_{21}) \frac{\hat{M}_{10}}{\hat{L}_1^{\text{eff}}} \end{aligned} \quad (37)$$

and $\Gamma\tau_2$ is the growth rate of the RWM in the absence of the active feedback circuit (Eq. (26)). From Eq. (37) it can be seen that the kink mode

can be completely stabilized by TF feedback if the numerator can be made negative. The factor $\hat{M}_{30} - \hat{M}_{31}\hat{M}_{10}/\hat{L}_1^{\text{eff}}$ is therefore the key: for fixed locations of the passive shell and active coil, this factor is negative if the flux measurements are made within some critical radius which depends on the value of \hat{L}_1^{eff} (Section 7). The sum of terms in \mathcal{A} in the denominator of Eq. (37) is positive. Therefore, if the sign of the gain, G_t , is chosen to be negative and its magnitude exceeds some critical value, the kink mode can be stabilized.

Figures 6 and 7 show root locus plots for feedback using the TF feedback scheme. The behaviour of the roots of the dispersion relation is shown for two assumed locations of the flux sensors. As before, $r_2/r_1 = 1.20$, $r_3/r_1 = 1.30$, $f = 0.6$ and $\beta^0 = 1.0$.

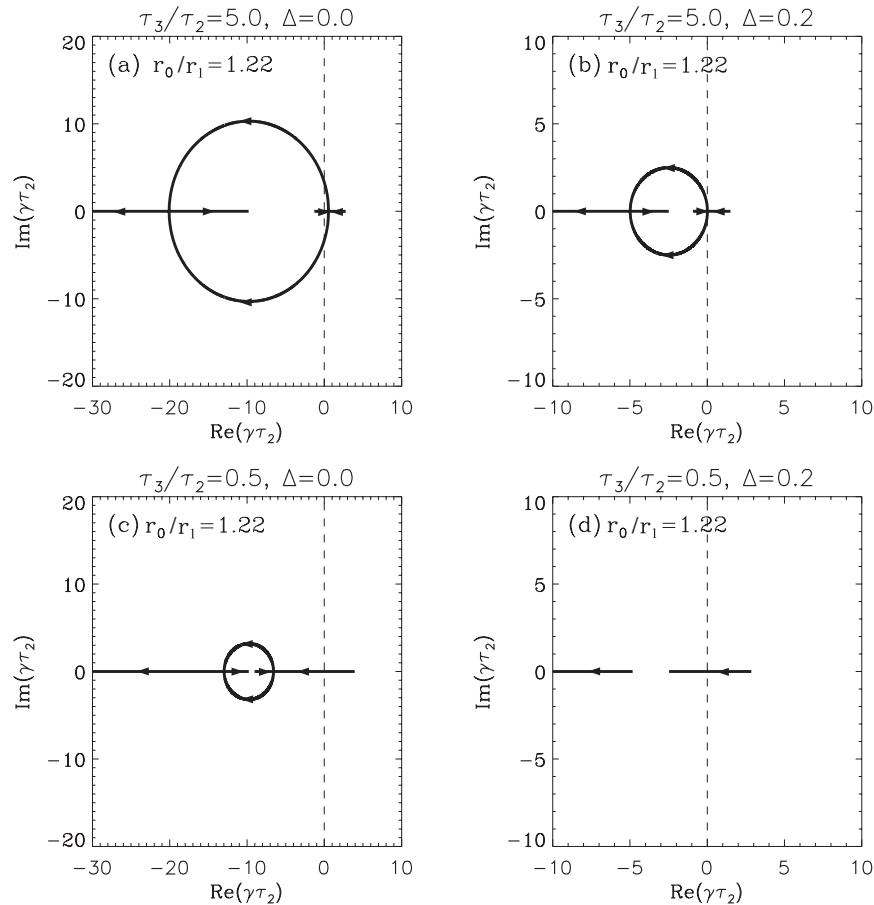


FIG. 6. Root locus plots for the TF feedback scheme. The plasma parameters are $f = 0.6$, $\beta^0 = 1.0$; the passive shell and active coil locations with respect to the plasma surface are $r_2/r_1 = 1.20$ and $r_3/r_1 = 1.30$, respectively. The flux sensor location is $r_0/r_1 = 1.22$. With sufficient gain, the unstable RWM root is damped. However, a significant oscillation frequency may be obtained, especially for large τ_3/τ_2 .

For a sensor location of $r_0/r_1 = 1.22$ (Fig. 6), the unstable root is stabilized if the gain is sufficiently large. When the time constant ratio is $\tau_3/\tau_2 = 5.0$, significant mode oscillation is induced (cf. ED feedback, Fig. 3(b)). If the time constant ratio is lowered, the critical damping rate at which oscillation first occurs is increased, and the maximum oscillation frequency is lowered. If the flux sensor is placed at a greater radius, say $r_0/r_1 = 1.26$ (Fig. 7), the initially unstable RWM root remains unstable for all values of the gain. The unstable growth rate does not approach zero as $G_t \rightarrow -\infty$, although for this value of the sensor location the magnitude of the unstable growth rate becomes a fraction of the inverse wall time. In this limit for the gain the stable growth rate approaches negative infinity along the real axis.

6.4. Fake rotating shell feedback

In common with TF feedback, for this feedback scheme it is assumed that the voltage acts in response to flux measurements made at radius $r = r_0$. The sensor location is shifted poloidally with respect to the feedback actuator providing a phase shift between the measured flux and the feedback voltage [14, 15]. The voltage appearing in Eq. (25) is written as

$$V_3\tau_3 = \text{im } G_f(M_{10}I_1 + M_{20}I_2 + M_{30}I_3). \quad (38)$$

The essential difference between the FRS feedback scheme and the TF scheme of the previous section is the $\sqrt{-1}$ multiplying the gain coefficient.

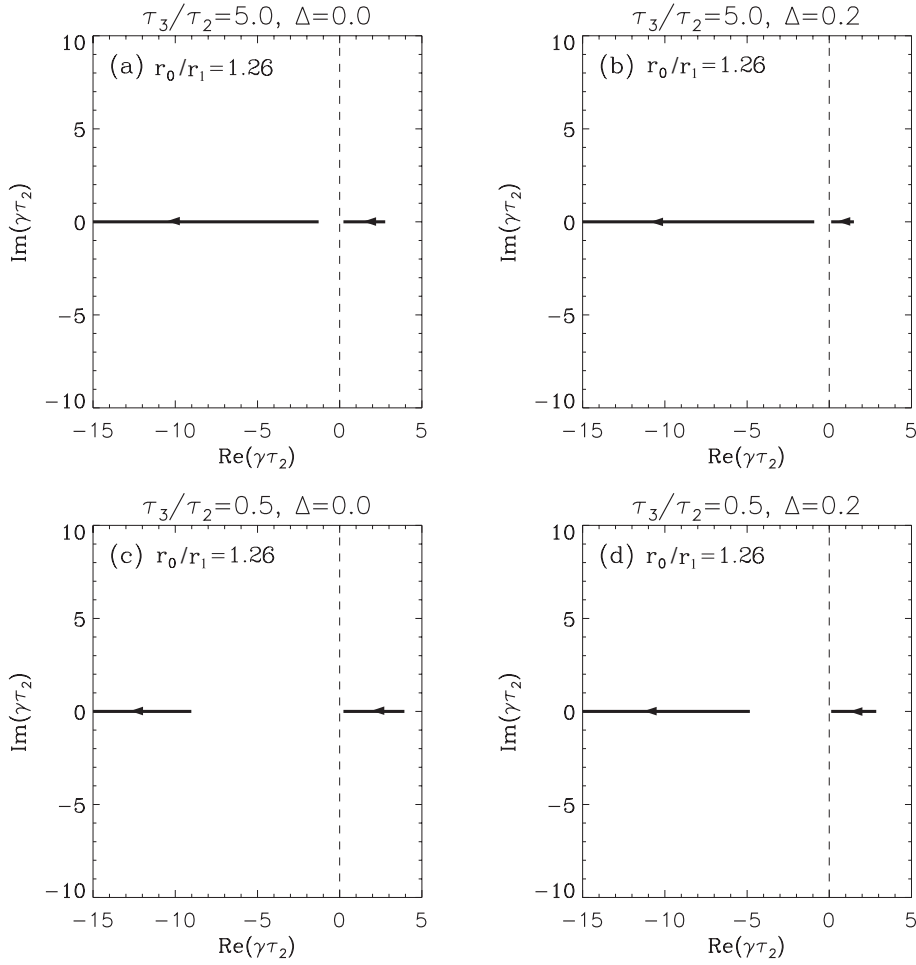


FIG. 7. Root locus plots for the TF feedback scheme with a flux sensor location of $r_0/r_1 = 1.26$. These should be contrasted with the plots shown in Fig. 6, where the flux sensor was at a smaller radius.

If $\tau_3 \ll \tau_2$ the solution corresponding to the dominant root is (Appendix B)

$$\gamma\tau_2 \approx \frac{1 - \text{im} G_f \left(\hat{M}_{30} - \frac{\hat{M}_{31}\hat{M}_{10}}{\hat{L}_1^{\text{eff}}} \right)}{\frac{1}{\Gamma\tau_2} - \text{im} G_f \mathcal{A}} \quad (39)$$

where $\Gamma\tau_2$ is the growth rate of the RWM in the absence of the active feedback circuit (Eq. (26)). Since this (complex) growth rate is of the form

$$\gamma\tau_2 = \frac{1 - iaG_f}{\frac{1}{\Gamma\tau_2} - ibG_f} \quad (40)$$

stability requires

$$\text{Re}(\gamma\tau_2) < 0 \Rightarrow \frac{1}{\Gamma\tau_2} + abG_f^2 < 0.$$

Since $\Gamma\tau_2 > 0$, a necessary condition for stability is $abG_f^2 < 0$, which implies that

$$\left(\hat{M}_{30} - \frac{\hat{M}_{31}\hat{M}_{10}}{\hat{L}_1^{\text{eff}}} \right) \mathcal{A} < 0 \quad (41)$$

independently of the sign of the gain G_f . For fixed locations of the passive and active circuits, this equation provides a necessary condition on the location of the observation points used in the feedback system. A sufficient condition for stability, assuming $\tau_3 \ll \tau_2$, is

$$\left(\hat{M}_{30} - \frac{\hat{M}_{31}\hat{M}_{10}}{\hat{L}_1^{\text{eff}}} \right) \mathcal{A} < -\frac{1}{m^2\Gamma\tau_2 G_f^2}. \quad (42)$$

An interesting feature of this scheme is the insensitivity of the feedback to the sign of the gain. As seen in Eq. (42), the gain appears as G_f^2 . This is in contrast to the other schemes, where the gain appears linearly.

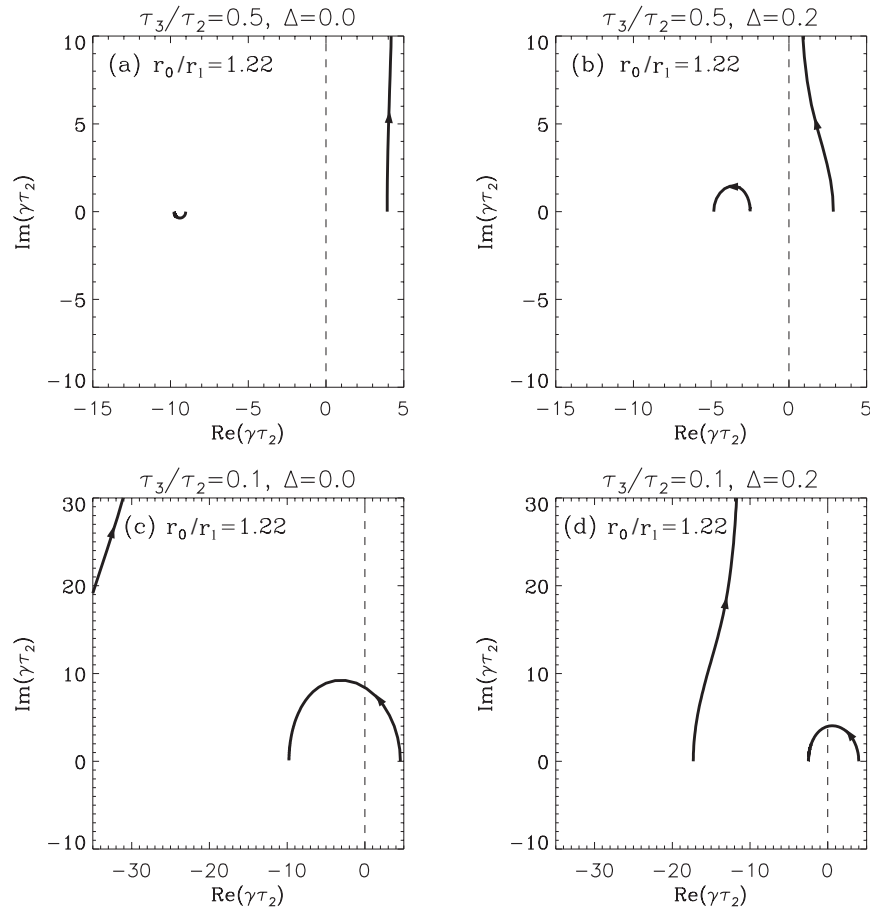


FIG. 8. Root locus plots for the FRS feedback scheme with $r_0/r_1 = 1.22$. Mode damping is achieved only if τ_3/τ_2 is small. A large oscillation frequency is always obtained. Note that $\text{im}(\gamma\tau_2) \rightarrow \infty$ as $G_f \rightarrow \infty$.

Shielding by the passive shell is identical to the shielding that occurs in TF feedback. For effective FRS feedback the flux at the observation point produced through the interaction with the plasma response, $(M_{31}I_3/L_1^{\text{eff}})M_{10}$, must be stronger than the direct flux, $M_{30}I_3$.

Figures 8 and 9 show root locus plots for feedback using the FRS feedback scheme. The behaviour of the roots of the dispersion relation is shown for plasma parameters $f = 0.6$, $\beta^0 = 1.0$, and for passive shell and active coil locations of $r_2/r_1 = 1.20$ and $r_3/r_1 = 1.30$, respectively. The figures show the results for $\tau_3/\tau_2 = 0.5$ and 0.1 . For the FRS feedback scheme to stabilize the kink mode the time constant ratio, τ_3/τ_2 , must be small (no stabilization is found for $\tau_3/\tau_2 = 0.5$), and the flux observation point must be sufficiently close to the plasma. Stabilization is seen in Figs 8(c) and (d) for $\tau_3/\tau_2 = 0.1$

and $r_0/r_1 = 1.22$. If $r_0/r_1 = 1.26$, however, no stabilization is achieved (Fig. 9). The FRS feedback characteristics are prone to oscillation since one of the roots satisfies $\text{im}(\gamma\tau_2) \rightarrow \infty$ as $G_f \rightarrow \infty$.

7. THE ISSUE OF SENSOR LOOP LOCATION

The TF and FRS feedback schemes rely on flux measurements at the radius r_0 . Root locus plots for these schemes show that the choice of r_0 , for a given f and τ_3/τ_2 , can determine whether or not a given kink mode can be stabilized. In this section, we determine the stable and unstable regions for placement of the sensor loop as a function of the plasma drive parameter $f = m - nq_a$, for different assumed values of the time constant ratio τ_3/τ_2 . We assume $\beta^0 = 1.0$, $r_2/r_1 = 1.20$ and $r_3/r_1 = 1.30$. Stability requires $\text{Re}(\gamma) < 0$ for finite $\text{im}(\gamma)$ at finite gain.

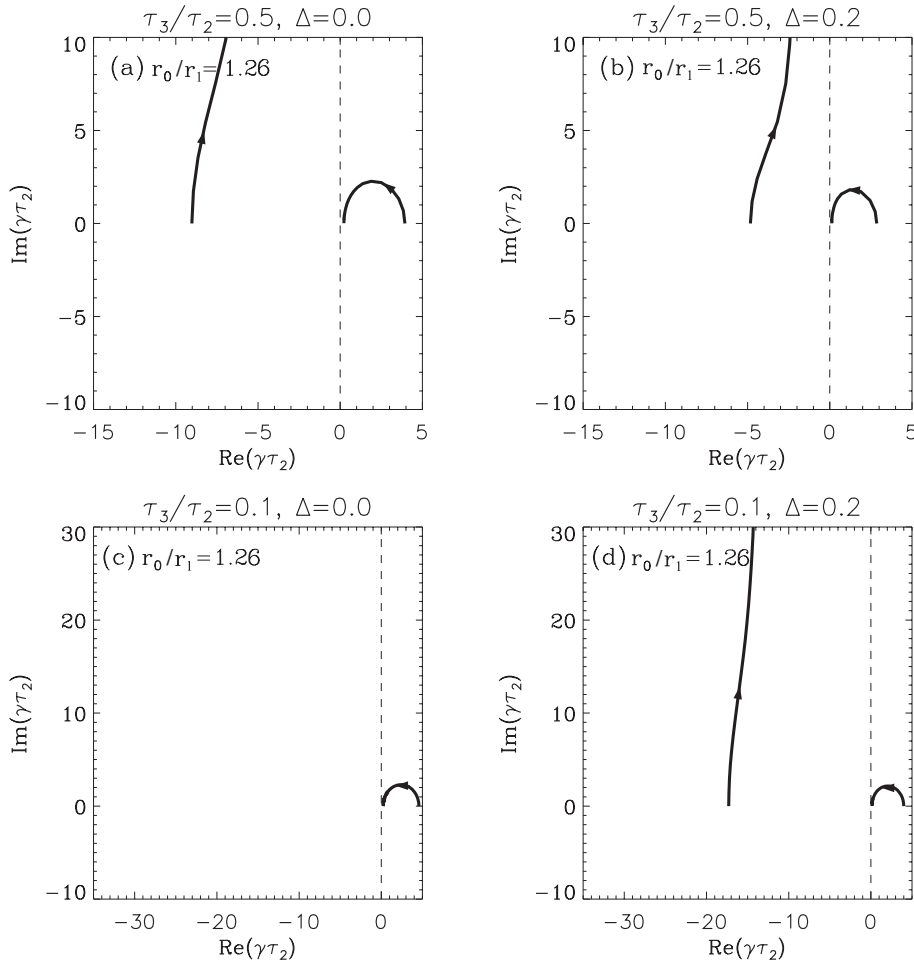


FIG. 9. Root locus plots for the FRS feedback scheme with $r_0/r_1 = 1.26$. This placement of the flux sensor is too distant from the plasma to stabilize the kink mode.

A stability diagram for the FRS scheme is shown in Fig. 10(a). The shaded region in the figure is the stable region for placement of the sensor loops assuming $\tau_3/\tau_2 = 1.0$. If τ_3/τ_2 is decreased, for example, to 0.1, the range of values of f that can be stabilized increases, as does the size of the window at fixed f . The upper boundary of the stable region, representing the maximum r_0 for a given f , is determined by the condition $\hat{M}_{30} - \hat{M}_{31}\hat{M}_{10}/\hat{L}_1^{\text{eff}} = 0$, and is achieved only at infinite gain. This boundary is independent of the value of τ_3/τ_2 . The lower boundary, representing the minimum r_0 for stability, is independent of f and depends on the value of τ_3/τ_2 . Stable and unstable regions for the TF feedback scheme are shown in Fig. 10(b). The shaded area is the stable region for $\tau_3/\tau_2 = 1.0$. For any value of τ_3/τ_2 , and $f > f_\tau = [(1 - \hat{M}_{21}\hat{M}_{12}) + \tau_3/\tau_2(1 - \hat{M}_{31}\hat{M}_{13})]/(1 + \tau_3/\tau_2)$,

the minimum sensor radius for which stability can be achieved is $r_0 = r_1$, the plasma radius. For more unstable plasmas, with $f < f_\tau$, the minimum r_0 is the shell radius, $r_0 = r_2$. A comparison between Figs 10(a) and (b) clearly shows that the TF scheme is more forgiving with respect to the placement of sensor loops than is the FRS scheme.

8. TIME RESPONSE OF THE FEEDBACK SCHEMES

The stable/unstable boundaries shown in Fig. 10 correspond to infinite gain solutions of the dispersion relation. In the practical implementation of a feedback scheme we are limited to finite gain scenarios. In this section we display time histories of the

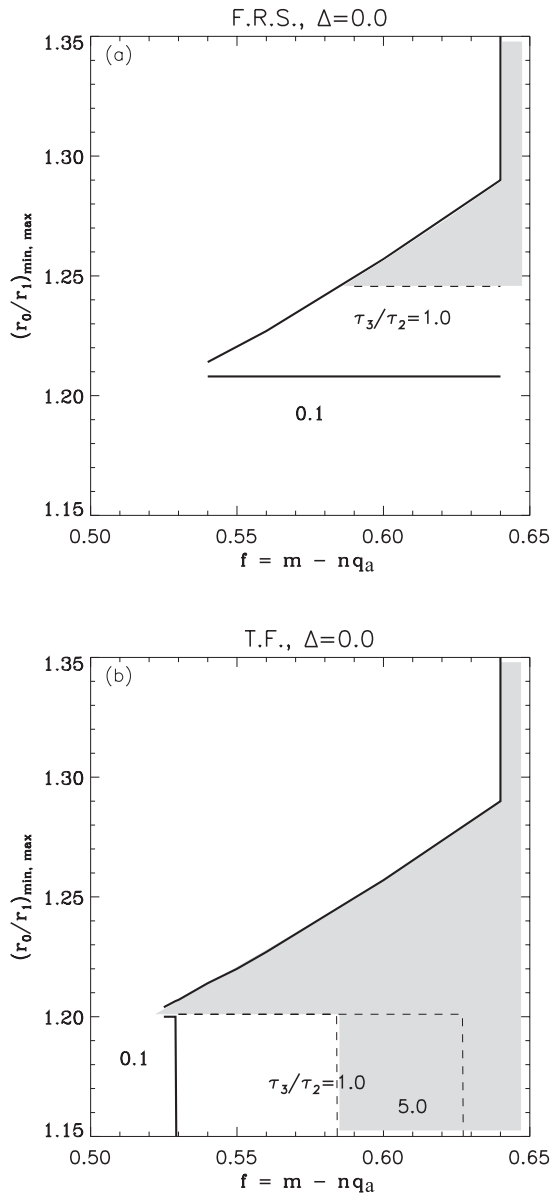


FIG. 10. Stable and unstable regions for placement of sensor loops for (a) the FRS and (b) the TF feedback systems. For any value of f , there is a stable window for placement of r_0 whose width depends on the assumed value of τ_3/τ_2 . The shaded region in each of the figures corresponds to $\tau_3/\tau_2 = 1.0$.

perturbed plasma current, $I_1(t)$, for the various feedback schemes. Finite values for the gain coefficient G are used, and the abilities of the feedback schemes to suppress the mode amplitude are compared.

Figure 11 shows a plot of the time dependence of the perturbed plasma current using the SC feedback scheme. The plasma parameters are $f = 0.6$ and $\beta_0 = 1.0$. The resistive shell and feedback coil radii are $r_2/r_1 = 1.2$ and $r_3/r_1 = 1.3$, respectively, and the

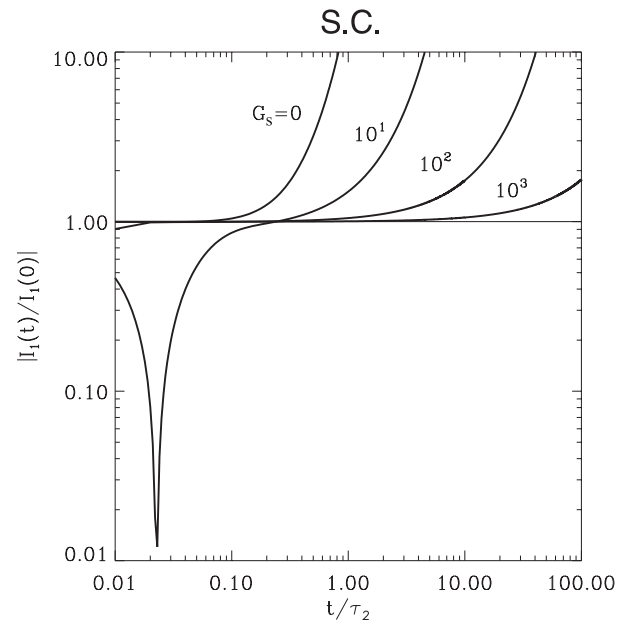


FIG. 11. Time dependence of the plasma circuit current, $I_1(t)$, using the SC feedback scheme. Each curve is labelled by the value of the gain, G_s . The plasma parameters are $f = 0.6$, $\beta^0 = 1.0$. The radii of the resistive shell and active feedback coils are $r_2/r_1 = 1.2$ and $r_3/r_1 = 1.3$, respectively. The ratio of time constants for the shell and active coil circuits is $\tau_3/\tau_2 = 1.0$.

ratio of time constants of the active and passive systems is $\tau_3/\tau_2 = 1.0$. The different curves are labelled by the value of the gain coefficient, G_s . Each curve is obtained from the response of the circuit equations, Eq. (59), to initial conditions with zero current in the feedback circuit, $I_3(0) = 0$, but finite current in the resistive shell. The curve labelled $G_s = 0$ shows exponential growth of the resistive wall mode without feedback. For $G_s = 10$ the kink mode amplitude initially decreases, overshoots $|I_1| = 0$, then increases without bound. (The absolute value of $I_1(t)$ is plotted; hence the appearance of the cusp as the amplitude goes through zero.) For larger values of the gain, G_s , the amplitude rapidly decreases, overshoots zero, then dwells near the initial value for a time interval that increases as the gain is increased. With an infinite gain, the amplitude can be maintained near the initial value for an infinite time, independently of the plasma and circuit parameters. The guaranteed improvement in the suppression of the mode growth with increasing G_s is a consequence of the asymptotic approach of the unstable root locus to $\text{Re}(\gamma) = 0$ seen in Fig. 5.

The following estimate shows that gain factor values of $G_s \sim 10^3$ – 10^4 are possible for a realistic

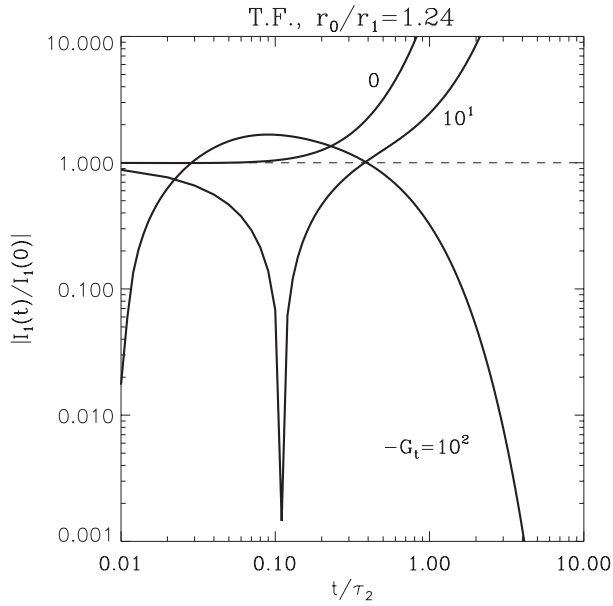


FIG. 12. Time dependence of the plasma circuit current, $I_1(t)$, using the TF feedback scheme with a flux sensor location of $r_0 = 1.24$, which is in the stable region of Fig. 10. The plasma and circuit parameters are the same as those in Fig. 11.

feedback scheme. Rearranging Eq. (33) for the voltage supplied to the feedback circuit gives

$$G_s = \frac{V_3}{I_2} \frac{\tau_3}{\tau_2} \frac{1}{R_2} \quad (43)$$

where the inductance L_2 has been eliminated in favour of $\tau_2 R_2$. Now interpret I_2 in this expression as a minimum detected current for which the feedback system is to respond with the maximum supplied voltage, V_3 . For a conservative estimate, assume $I_2 = 100$ A and $V_3 = 500$ V. Assume $\tau_3/\tau_2 = 1.0$. For the resistance of the passive shell, R_2 , use Eq. (14) with a poloidal mode number of $m = 2$, aspect ratio $R_0/r_1 = 3.0$, passive shell radius $r_2/r_1 = 1.2$ and a 1 cm thick stainless steel passive shell ($\eta = 11 \times 10^{-8} \Omega \cdot \text{m}$). The estimate is $G_s = 5 \times 10^4$. Thus, we see from Fig. 11 that employing the SC feedback scheme using realistic gain factors enables suppression of the kink mode amplitude for times that are very long compared with the L/R time constant of the passive shell.

Figure 12 shows a similar plot using the TF feedback scheme. The same plasma and circuit parameters are used for the TF simulation as were used for the SC simulation. The flux sensor was assumed to be at location $r_0/r_1 = 1.24$, which is in the stable region of the stability diagram, Fig. 10. We see that

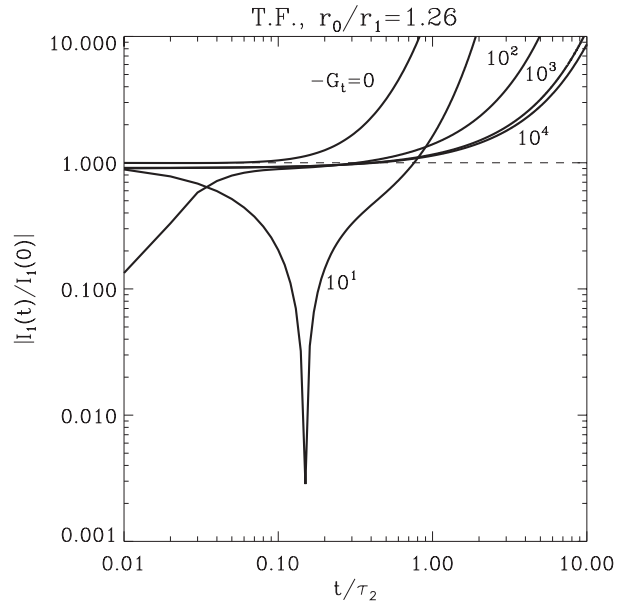


FIG. 13. Time dependence of the plasma circuit current, $I_1(t)$, using the TF feedback scheme with a flux sensor location of $r_0 = 1.26$. This is in the unstable region of Fig. 10. The plasma and circuit parameters are the same as those in Fig. 11.

for a gain of $G_t = -10$ the plasma mode amplitude initially decreases, but overshoots zero and increases without limit. For $G_t = -100$, although there is an initial overshoot, the mode amplitude is eventually driven towards zero. Figure 13 shows the behaviour of TF feedback when the sensor location is moved slightly beyond the edge of the stable region, to $r_0/r_1 = 1.26$. The behaviour of the mode amplitude is qualitatively similar to that in the SC scheme, except that the mode amplitude cannot be maintained near its initial value for arbitrary times. Even for infinitely large gain values, the resistive wall mode grows appreciably for $t \gtrsim \tau_2$. This is a consequence of the asymptotic approach of the unstable root locus to a finite $\text{Re}(\gamma) > 0$ as $G_t \rightarrow -\infty$, as seen in Fig. 7. Thus, if the TF feedback scheme is the feedback method of choice, the success of the feedback system in suppressing the kink mode depends critically on careful placement of the flux sensors.

9. FLUX COMPENSATION COEFFICIENT

Here, we introduce a useful parameter for determining the expected range of plasma profiles that can be stabilized by the SC and TF feedback schemes. This parameter, named the flux compensation

coefficient, C_ψ , is the ratio of the flux produced at the passive shell by the active coil to the sum of the fluxes due to the passive shell and the perturbed plasma current,

$$C_\psi = \frac{M_{32}I_3}{M_{12}I_1 + L_2I_2}. \quad (44)$$

If $C_\psi = -1$ the field due to the active coil instantaneously compensates 100% of the flux loss in the shell. The shell therefore acts as a perfect conductor and is guaranteed to stabilize the kink mode. Realistic feedback systems cannot achieve $C_\psi = -1$. For a feedback system operating with some given gain, C_ψ is a measure of the efficiency of the feedback scheme. An efficient feedback system will reduce the growth rate of the instability with a minimum amount of flux compensation.

An equation can be derived for the circuit equation growth rate in terms of the flux compensation coefficient. First, we rearrange the resistive wall circuit equation, Eq. (23), in the form

$$\gamma\tau_2 = \frac{I_2/I_3}{\frac{I_2}{I_3} \frac{1}{\Gamma\tau_2} - \left(\hat{M}_{23} - \frac{\hat{M}_{21}\hat{M}_{13}}{\hat{L}_1^{\text{eff}}} \right)}. \quad (45)$$

The flux compensation coefficient, C_ψ , can also be written in terms of the current ratio I_2/I_3 by eliminating I_1 from Eq. (44) using the plasma circuit equation, Eq. (23),

$$C_\psi = \frac{-\hat{M}_{23}}{\frac{I_2}{I_3} \frac{1}{\Gamma\tau_2} + \frac{\hat{M}_{21}\hat{M}_{13}}{\hat{L}_1^{\text{eff}}}}. \quad (46)$$

The circuit equation growth rate $\gamma\tau_2$, expressed in terms of C_ψ , is therefore

$$\frac{\gamma\tau_2}{\Gamma\tau_2} = 1 - \frac{C_\psi}{1 + C_\psi} \left(1 - \frac{\hat{M}_{21}\hat{M}_{13}/\hat{M}_{23}}{\hat{L}_1^{\text{eff}}} \right). \quad (47)$$

We see that for fixed resistive shell and active feedback coil locations, $\gamma\tau_2$ is a function of C_ψ and $\hat{L}_1^{\text{eff}}(f, \beta^0)$, but is independent of τ_3/τ_2 and r_0 . For a given plasma drive, the dependence of $\gamma\tau_2$ on C_ψ is independent of the details of the feedback scheme; it is the same for the SC, TF and FRS schemes.

In general, the flux compensation coefficient is a complex number. For the SC feedback scheme, C_ψ is real for all values of the gain G_s . For the TF scheme, C_ψ is real for all values of G_t unless the two roots of the dispersion relation coalesce. Whether or not there is a coalescence depends on the location of the

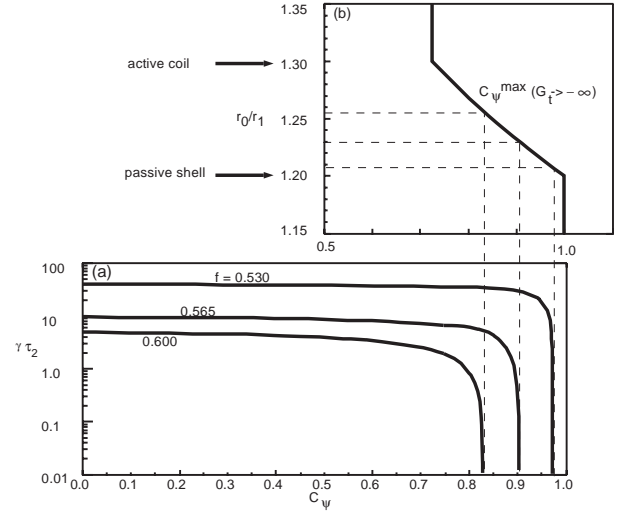


FIG. 14. (a) Feedback system growth rate, $\gamma\tau_2$, as a function of the flux compensation coefficient, C_ψ . Three curves are shown, labelled by the value of the plasma drive $f = m - nq_a$. The curves do not depend on the details of the feedback system, i.e. on τ_3/τ_2 or r_0/r_1 . (b) The dependence of the maximum achievable C_ψ (infinite gain limit) on flux sensor radius, r_0/r_1 .

flux sensor and on the value of τ_3/τ_2 (Fig. 6). If a coalescence occurs at $G_t = -G_t^{\text{crit}}$, C_ψ is real for $G_t^{\text{crit}} < G_t < 0$. For the FRS scheme, C_ψ is real only for $G_f = 0$ and $|G_f| = \infty$.

A plot of $\gamma\tau_2$ versus C_ψ is shown in Fig. 14(a) for three values of the plasma drive parameter, f , assuming $\beta^0 = 1.0$. The plot assumes that both $\gamma\tau_2$ and C_ψ are real and therefore applies only to the SC and TF feedback schemes. We now investigate what the minimum growth rate is that can be achieved by these feedback schemes. Since $\gamma\tau_2$ is monotonic in C_ψ , the answer is found by seeking the maximum value for the flux compensation coefficient for each of the feedback systems. To find this maximum we consider the infinite gain limit of the feedback circuit equation, Eq. (25). If the gain is infinite and the feedback system is to be effective, the circuit currents and the growth rate must remain finite. Therefore, the coefficient of G in the expression for $V_3\tau_3$ must vanish. For SC feedback, where $V_3\tau_3 = G_s L_2 I_2$, infinite gain implies that I_2 vanishes. Substituting $I_2/I_3 = 0$ in Eq. (46), and the resulting expression for C_ψ^{max} into Eq. (47), yields $\gamma\tau_2 = 0$ for the minimum growth rate achievable using SC feedback for any plasma drive. This, of course, agrees with the root locus plot discussion in Section 6.2. For the TF feedback scheme, the condition on $V_3\tau_3$ at infinite gain implies that

$M_{10}I_1 + M_{20}I_2 + M_{30}I_3 = 0$. Eliminating I_1 in terms of I_2 and I_3 using the plasma circuit equation leads to

$$I_2/I_3 = -(M_{30} - M_{31}M_{10}/L_1^{\text{eff}})/(M_{20} - M_{21}M_{10}/L_1^{\text{eff}}).$$

Substitution into Eq. (46) leads to an expression for C_ψ^{max} . Since I_2/I_3 depends on the mutual inductances M_{j0} , C_ψ^{max} depends on the location of the flux sensor. Using the cylindrical limit expressions for the M_{j0} , a plot of sensor radius r_0/r_1 versus C_ψ^{max} is obtained (Fig. 14(b)). Three dashed lines are drawn, corresponding to sensor locations that can completely stabilize plasmas with $f = 0.600$, $f = 0.565$ and $f = 0.530$. If the sensor is placed at $r_0/r_1 = 1.23$, Fig. 14 shows that infinite gain implies a flux compensation coefficient of $C_\psi = -0.90$. The figure also shows that plasmas with $f > 0.565$ can be stabilized by the TF scheme using infinite gain. However, if $f = 0.530$ the feedback system is ineffective at reducing the growth rate with this sensor loop no matter how large a gain is used.

Although, with infinite gain, the SC method can reduce the RWM growth rate to zero for any plasma profile, we must accept that system noise and discreteness of the feedback coil design will limit the reduction in flux at the resistive wall. Prototype feedback circuits have been designed and tested for reducing the fluctuating magnetic field normal to a square coil [29] and have shown reductions in the field of 90%, corresponding to a $C_\psi = -0.9$. Such a reduction is probably a realistic goal for a tokamak experiment with a discrete coil set. This upper limit on C_ψ sets a limit on the range of profiles a feedback system can expect to stabilize.

10. SUMMARY AND CONCLUSIONS

In this article we have introduced a circuit equation formulation for the feedback stabilization of RWMs in tokamaks. The formalism is analogous to the circuit equation approaches commonly used for the design and analysis of $n = 0$ control systems. Several feedback schemes have been discussed. The various schemes differ in the choice of sensor signal. Although the results presented in this article are limited to proportional feedback control, adding differential and integral feedback terms leads to a straightforward modification of the present analysis (e.g., Ref. [28]). These additional terms can sometimes improve the system response. However, as a

matter of overall feedback design philosophy, our preference is to seek a basically stable system with proportional control alone and regard the differential and integral control terms as correction terms.

The SC scheme assumes that the voltage supplied to the feedback circuit is proportional to the measured eddy current flowing in the passive conducting shell. Although complete stabilization of an $n \geq 1$ kink mode is not possible with this scheme, the unstable growth rate can be made extremely small if the gain is large, effectively suppressing the RWM for times that are orders of magnitude longer than the time constant of the passive shell. For the SC scheme, the roots of the RWM dispersion relation are purely real. This is an advantage over other schemes discussed in this article; oscillatory characteristics of a feedback system can be problematic if the plasma MHD mode frequency coincides with the feedback system oscillation frequency.

The TF and FRS feedback schemes rely on local measurements of the total perturbed flux. They have the potential advantage over the SC scheme of being able to completely stabilize the kink mode. Both of these schemes show oscillatory feedback characteristics. The ‘correct’ placement of the flux sensors is also an issue for these schemes. This is especially true for the FRS scheme, which does not allow placement of the sensors near the passive shell unless the ratio of time constants for the passive shell and active coil systems, τ_3/τ_2 , is small.

The present analysis is valid in the cylindrical limit of infinite aspect ratio where a single m/n helicity is present. For generalization to toroidal configurations, a critical factor is whether a single helicity remains dominant. For the $n = 0$ instability there is a dominant quasi-uniform radial magnetic field pattern at the plasma surface and at the passive shell. This quasi-uniform B_R pattern can be easily produced by a simple active coil arrangement. For $n \geq 1$, the normal magnetic field pattern due to the plasma perturbation can have a rich poloidal spectrum at the plasma surface. However, this spectrum looks remarkably simple when evaluated at the surface of a perfectly conducting shell [29] near conditions of marginal stability. A feedback coil system that seeks to make the total normal magnetic field at the passive shell vanish and make the passive shell appear to be perfectly conducting need only produce the negative of this simple field pattern. Details of RWM stabilization in fully toroidal geometry remain to be investigated.

The present circuit equation approach to resistive wall mode feedback control suggests the possibility

of building a three dimensional hardware simulator to test feedback control strategies in realistic geometry. This would be an important extension of the hardware simulator of Platt and Robertson [30], who used an idealized geometry. The present formulation shows the possibility of including a plasma circuit whose inductance can be varied to simulate a variety of plasma profiles. Such a simulator would be a cost effective method for exploring the efficacy of kink mode control on advanced tokomaks.

Appendix A

DERIVATION OF CIRCUIT SELF-INDUCTANCE AND MUTUAL INDUCTANCES

From the requirement of continuity of the total perturbed pressure across the perturbed plasma–boundary interface, we easily derive

$$[a/B_\theta^0(a)]B_\theta^{\text{vac}}(a) = if\xi_\theta(a) \quad (48)$$

where $B_\theta^{\text{vac}}(a)$ is the perturbed vacuum poloidal field evaluated at the unperturbed plasma edge. The poloidal field is imagined to be generated by helical current filaments wrapped on a toroidal surface with major radius $R = R_0$ and minor radius $r = a$. The current in each filament is

$$I_1 = \frac{2\pi a}{m} B_\theta^{\text{vac}}(a_+). \quad (49)$$

Using the radial projection of Faraday’s law,

$$[a/B_\theta^0(a)]B_r = i\hat{F}\xi_r \quad (50)$$

continuity of B_r across the plasma–vacuum interface and Eq. (4) to replace B_r in terms of the poloidal flux ψ leads to

$$I_1 = \psi/R_0. \quad (51)$$

The self-inductance of a circuit is defined through the relationship of the poloidal flux due to the current in the circuit, and the current carried by the circuit, where the flux is evaluated at the location of the circuit. Thus, for circuit ‘ i ’,

$$\psi(r = r_i) = L_i I_i. \quad (52)$$

From Eq. (51), we therefore identify

$$L_1 = R_0. \quad (53)$$

Since the poloidal flux in the vacuum region due to the isolated plasma circuit is $\psi \sim r^{-m}$, $\psi'(a_+) = -(m/a)\psi(a_+)$ and therefore

$$L'_1 = -(m/a)L_1. \quad (54)$$

Similarly, the mutual inductance between circuits ‘ i ’ and ‘ j ’ is defined in terms of the flux at the location of circuit ‘ j ’ due to a current in circuit ‘ i ’,

$$\psi(j) = M_{ij} I_i. \quad (55)$$

In the cylindrical limit,

$$\psi(i) \propto (r_i/r_j)^m, \quad r_i < r_j \quad (56a)$$

$$\psi(i) \propto (r_j/r_i)^m, \quad r_i > r_j. \quad (56b)$$

Also, as $r_j \rightarrow r_i$, $M_{ij} \rightarrow L_i$. Thus,

$$M_{ij} = R_0(r_i/r_j)^m, \quad r_i < r_j \quad (57a)$$

$$M_{ij} = R_0(r_j/r_i)^m, \quad r_i > r_j. \quad (57b)$$

Appendix B

DETAILS OF THE DERIVATION OF THE CIRCUIT DISPERSION RELATION

The circuit equations describing the interaction of a feedback circuit with a resistive wall mode are Eqs (23)–(25). The feedback voltage \mathbf{V} can in general be written as the product of a gain factor, G , and an observed flux to feedback,

$$\begin{aligned} V_3\tau_3 &= G\psi(\text{at obs. location}) \\ &= G(M_{10}I_1 + M_{20}I_2 + M_{30}I_3). \end{aligned} \quad (58)$$

For the ED feedback scheme we keep only the term which multiplies I_1 and set $G_1 = G_e L_1 I_1$ (Section 6.1). For the SC scheme we keep only the term with I_2 and set $G_2 = G_s L_2 I_2$ (Section 6.2). For the FRS scheme we keep all terms and set $G_1 = G_2 = G_3 = \text{Im } G_f$ (Section 6.4).

Using Eq. (23), we eliminate I_1 from Eqs (24) and (25), and obtain dynamical circuit equations for the passive shell and active feedback circuits in the form

$$\tilde{\mathbf{M}} \frac{\partial \mathbf{I}}{\partial t} + \mathbf{R} \mathbf{I} = \tilde{\mathbf{V}} \quad (59)$$

where

$$\tilde{\mathbf{M}} = \begin{pmatrix} \tilde{L}_2 & \tilde{M}_{23} \\ \tilde{M}_{32} & \tilde{L}_3 \end{pmatrix}, \quad \mathbf{R} = \begin{pmatrix} R_2 & 0 \\ 0 & R_3 \end{pmatrix} \quad (60)$$

$$\tilde{\mathbf{V}} = \begin{pmatrix} 0 \\ \tilde{V}_3 \end{pmatrix} \quad \text{and} \quad \mathbf{I} = \begin{pmatrix} I_2 \\ I_3 \end{pmatrix}. \quad (61)$$

Here,

$$\tilde{V}_3\tau_3 = G(\tilde{M}_{20}I_2 + \tilde{M}_{30}I_3) \quad (62)$$

$$\tilde{L}_i = \tilde{M}_{ii} \quad (63)$$

and \tilde{M}_{ij} are ‘dressed inductances’ defined by

$$\tilde{M}_{ij} = M_{ij} - \frac{M_{i1}M_{1j}}{L_1^{\text{eff}}}. \quad (64)$$

The Laplace transform of Eq. (59) is

$$\mathbf{I}(\gamma) = \tau_2 \frac{\mathbf{N}(\gamma)}{D(\gamma)} \mathbf{I}(0) \quad (65)$$

where the transfer matrix elements, N_{ij} , are

$$\begin{aligned} N_{11} = & (\gamma\tau_3) \left[\frac{1}{\Gamma\tau_2} + (\hat{M}_{31} - \hat{M}_{32}\hat{M}_{21}) \frac{\hat{M}_{13}}{\hat{L}_1^{\text{eff}}} \right. \\ & \left. + \left(\hat{M}_{32} - \frac{\hat{M}_{31}\hat{M}_{12}}{\hat{L}_1^{\text{eff}}} \right) \hat{M}_{23} \right] \\ & + \frac{1}{\Gamma\tau_2} \left[1 - G \left(\hat{M}_{30} - \frac{\hat{M}_{31}\hat{M}_{10}}{\hat{L}_1^{\text{eff}}} \right) \right] \end{aligned}$$

$$\begin{aligned} N_{12} = & - \left(\hat{M}_{23} - \frac{\hat{M}_{21}\hat{M}_{13}}{\hat{L}_1^{\text{eff}}} \right) \\ & \times \left[1 - G \left(\hat{M}_{30} - \frac{\hat{M}_{31}\hat{M}_{10}}{\hat{L}_1^{\text{eff}}} \right) \right] \end{aligned}$$

$$\begin{aligned} N_{21} = & - \frac{L_2}{L_3} \left[\left(\hat{M}_{23} - \frac{\hat{M}_{21}\hat{M}_{13}}{\hat{L}_1^{\text{eff}}} \right) \right. \\ & \left. - \frac{G}{\Gamma\tau_2} \left(\hat{M}_{20} - \frac{\hat{M}_{21}\hat{M}_{10}}{\hat{L}_1^{\text{eff}}} \right) \right] \end{aligned}$$

$$\begin{aligned} N_{22} = & (\gamma\tau_3) \left[\frac{1}{\Gamma\tau_2} + (\hat{M}_{31} - \hat{M}_{32}\hat{M}_{21}) \frac{\hat{M}_{13}}{\hat{L}_1^{\text{eff}}} \right. \\ & \left. + \left(\hat{M}_{32} - \frac{\hat{M}_{31}\hat{M}_{12}}{\hat{L}_1^{\text{eff}}} \right) \hat{M}_{23} \right] - \left(1 - \frac{\hat{M}_{31}\hat{M}_{13}}{\hat{L}_1^{\text{eff}}} \right) \\ & - G \left(\hat{M}_{20} - \hat{M}_{21}\hat{M}_{10} \right) \left(\hat{M}_{32} - \frac{\hat{M}_{31}\hat{M}_{12}}{\hat{L}_1^{\text{eff}}} \right) \quad (66) \end{aligned}$$

and the denominator is

$$\begin{aligned} D(\gamma) = & (\gamma\tau_2)(\gamma\tau_3) \left[\frac{1}{\Gamma\tau_2} + \left(\hat{M}_{32} - \frac{\hat{M}_{31}\hat{M}_{12}}{\hat{L}_1^{\text{eff}}} \right) \hat{M}_{32} \right. \\ & \left. + \left(\hat{M}_{31} - \hat{M}_{32}\hat{M}_{21} \right) \frac{\hat{M}_{13}}{\hat{L}_1^{\text{eff}}} \right] \\ & + (\gamma\tau_2) \left\{ \frac{1}{\Gamma\tau_2} - G \left[\frac{\hat{M}_{30}}{\Gamma\tau_2} \right. \right. \\ & \left. \left. + \left(\hat{M}_{32} - \frac{\hat{M}_{31}\hat{M}_{12}}{\hat{L}_1^{\text{eff}}} \right) \hat{M}_{20} \right. \right. \\ & \left. \left. + \left(\hat{M}_{31} - \hat{M}_{32}\hat{M}_{21} \right) \frac{\hat{M}_{10}}{\hat{L}_1^{\text{eff}}} \right] \right\} \\ & - (\gamma\tau_3) \left[1 - \frac{\hat{M}_{31}\hat{M}_{13}}{\hat{L}_1^{\text{eff}}} \right] \\ & - \left[1 - G \left(\hat{M}_{30} - \frac{\hat{M}_{31}\hat{M}_{10}}{\hat{L}_1^{\text{eff}}} \right) \right]. \quad (67) \end{aligned}$$

The characteristic equation defining the growth rates of the linear feedback equations is $D(\gamma) = 0$. This quadratic equation has the form

$$\gamma^2(a\tau_3\tau_2) + \gamma(b\tau_3 + c\tau_2) + d = 0. \quad (68)$$

The condition for complex roots is

$$(b\tau_3/\tau_2 + c)^2 - 4ad\tau_3/\tau_2 < 0. \quad (69)$$

For SC feedback we note that $d < 0$. This is the only feedback scheme that guarantees purely real growth rates, independent of the value of the gain or time constants of the passive and active feedback systems.

Assuming that the L/R time for the active circuit is much slower than that of the passive circuit (i.e. $\tau_3 \ll \tau_2$), the two roots of Eq. (68) are $\gamma\tau_2 \approx -d/c$ and $\gamma\tau_2 \approx -c\tau_2/a\tau_3$. The first of these is the more unstable root and is given by

$$\gamma\tau_2 = \frac{1 - G \left(\hat{M}_{30} - \frac{\hat{M}_{31}\hat{M}_{10}}{\hat{L}_1^{\text{eff}}} \right)}{\frac{1}{\Gamma\tau_2} - G\mathcal{A}} \quad (70)$$

where

$$\begin{aligned} \mathcal{A} = & \frac{\hat{M}_{30}}{\Gamma\tau_2} + \hat{M}_{20} \left(\hat{M}_{32} - \frac{\hat{M}_{31}\hat{M}_{12}}{\hat{L}_1^{\text{eff}}} \right) \\ & + \left(\hat{M}_{31} - \hat{M}_{32}\hat{M}_{21} \right) \frac{\hat{M}_{10}}{\hat{L}_1^{\text{eff}}}. \end{aligned}$$

By substituting the appropriate expression for the gain, G , the SC, FRS and ED dispersion relations (Eqs (34), (39) and (31)) are obtained.

It is interesting to note that the expression, Eq. (70), for the case of SC feedback is identical to that obtained if $V_3\tau_3 = G_s L_2 I_2$ is replaced by the current feedback law, $I_3 = G_s I_2$. The algebra for this case is trivial, since the solution of Eqs (23) and (24) with this restriction on I_3 is linear in the growth rate.

ACKNOWLEDGEMENTS

We are indebted to R. Woolley who raised with us the need for the type of analysis presented in this article, and we are pleased to acknowledge useful discussions with M. Chance and S.C. Jardin. This research was sponsored by the Office of Fusion Energy Science, USDOE, under Contract No. DE-AC05-84OR21400.

REFERENCES

- [1] YOSHINO, R., et al., Fusion Technol. **30** (1996) 237.
- [2] NAKAMURA, Y., et al., Nucl. Fusion **36** (1996) 643.
- [3] TANGA, A., et al., in Fusion Engineering (Proc. 13th Symp. Knoxville, 1989), Vol. 2, IEEE, New York (1989) 1271.
- [4] LAZARUS, E.A., LISTER, J.B., NEILSON, G.H., Nucl. Fusion **30** (1990) 111.
- [5] LISTER, J.B., et al., Nucl. Fusion **30** (1990) 2349.
- [6] GRUBER, O., et al., Plasma Phys. Control. Fusion **35** (1993) B191.
- [7] HUTCHINSON, I.H., et al., Fusion Technol. **30** (1996) 137.
- [8] HATCHER, R., OKABAYASHI, M., Integrated Shell Approach to Vertical Position Control on PBX-M, Rep. 3089, Princeton Plasma Phys. Lab., NJ (1995).
- [9] STRAIT, E.T., et al., Phys. Plasmas **1** (1994) 1415.
- [10] TAYLOR, T., et al., Phys. Plasmas **2** (1995) 2390.
- [11] OKABAYASHI, M., et al., Nucl. Fusion **36** (1996) 1167.
- [12] FREIDBURG, J.P., Ideal Magnetohydrodynamics, Plenum Press, New York (1987).
- [13] BISHOP, C.M., Plasma Phys. Control. Fusion **31** (1989) 1179.
- [14] FITZPATRICK, R., JENSEN, T.H., Phys. Plasmas **3** (1996) 2641.
- [15] JENSEN, T.H., FITZPATRICK R., Phys. Plasmas **4** (1997) 2997.
- [16] GIMBLETT, C.G., Plasma Phys. Control. Fusion **31** (1989) 2183.
- [17] BONDESON, A., WARD, D.J., Phys. Rev. Lett. **72** (1994) 2709.
- [18] POMPHREY, N., et al., in Plasma Physics and Controlled Nuclear Fusion Research 1994 (Proc. 15th Int. Conf. Seville, 1994), Vol. 3, IAEA, Vienna (1996) 251.
- [19] FITZPATRICK, R., AYDEMIR, A.Y., Nucl. Fusion **36** (1996) 11.
- [20] BOOZER, A.H., Phys. Plasmas **2** (1995) 4521.
- [21] OKABAYASHI, M., et al., "A filament model for resistive wall mode feedback stabilization", paper presented at the International Sherwood Fusion Theory Conf. Madison, 1997, paper 1C16.
- [22] HATCHER, R., et al., in Fusion Engineering (Proc. 17th Symp. San Diego, 1997), IEEE, Piscataway, NJ (1997).
- [23] BOOZER, A.H., Phys. Plasmas **5** (1998) 3350.
- [24] HAIN, K., LUST, R., Z. Naturforsch. **13a** (1958) 936.
- [25] WESSON, J., Nucl. Fusion **18** (1978) 87.
- [26] GRANETZ, R.S., MIT, Cambridge, MA, personal communication.
- [27] LAZARUS, E.A., Oak Ridge Natl Lab., TN, personal communication.
- [28] KUO, B.C., Automatic Control Systems, Prentice-Hall, Englewood Cliffs, NJ (1975).
- [29] PLATT, C.L., ROBERTSON, S.H., IEEE Trans. Plasma Sci. **19** (1991) 954.
- [30] LEE, D.Y., et al., Phys. Plasmas **5** (1998) 735.

(Manuscript received 23 April 1998
Final manuscript accepted 30 July 1998)

E-mail address of N. Pomphrey:
pomphrey@pppl.gov

Subject classification: E0, Tt; C0, Tt